Eur. Phys. J. B **58**, 11–23 (2007)
DOI: 10.1140/epjb/e2007-00204-6

THE EUROPEAN PHYSICAL JOURNAL B

# Helimagnetism in gallium substituted $LuMn_6Ge_6$ studied by nuclear magnetic resonance

J. Schnelzer[1], R. Montbrun[1], B. Pilawa[1], G. Fischer[1], G. Venturini[2], and E. Dormann[1,a]

[1] Physikalisches Institut, Universität Karlsruhe (TH), 76128 Karlsruhe, Germany
[2] Laboratoire de Chimie du Solide Minéral, Université Henri Poincaré-Nancy I, 54506 Nancy, France

Received 30 April 2007
Published online 28 July 2007 – © EDP Sciences, Società Italiana di Fisica, Springer-Verlag 2007

**Abstract.** Zero-field nuclear magnetic resonance (NMR) of all NMR isotopes ($^{175}$Lu, $^{55}$Mn, $^{73}$Ge, $^{69,71}$Ga) in $LuMn_6Ge_{6-x}Ga_x$, $0 \leq x \leq 1$, is used to monitor the variation of the hyperfine interaction with the sequence of antiferromagnetic - helimagnetic - ferromagnetic arrangement of the manganese moments of subsequent Kagomé net planes achieved by variation of the gallium content $x$. According to the $^{55}$Mn-NMR results, the local Mn moment varies by less than $\pm 5\%$ in this series. $^{175}$Lu-NMR proves canting of the antiferromagnetic sublattices in $LuMn_6Ge_6$. The anisotropy of the Ge magnetic hyperfine interaction decreases with increasing separation from the hexagonal Lu plane, whereas the absolute value of its isotropic part is only qualitatively correlated with the average separation of the six nearest Mn neighbours. Due to the anisotropic magnetic and electric hyperfine interaction at Ge and Ga sites, the non-collinear magnetic structures are clearly reflected by the NMR spectra, which are described quantitatively in this contribution. The preferred Mn moment direction rotates away from the $c$ direction with $x$. The conduction or bonding electron spin polarization at the Ga nuclei is increased by 35–80% compared to the Ge nuclei. We argue that this is related with the variation of the magnetic order with the Ga content.

**PACS.** 71.20.Lp intermetallic compounds – 75.25.+z Spin arrangement in magnetically ordered materials – 75.50.-y Studies of specific magnetic materials – 76.60.-k Nuclear magnetic resonance and relaxation – 76.60.Jx Effects of internal magnetic fields

## 1 Introduction

Manganese intermetallic compounds exhibit a fascinating variety of magnetic properties. The localized Mn magnetic moment disappears for small atomic volume and otherwise gives rise to various types of three-dimensionally ordered structures, including helical modulation with extremely long periods [1,2]. Sensitivity of these properties to temperature, external pressure or magnetic fields allows sensor applications using magnetoresistance based effects.

Ternary $RMn_6Ge_6$ intermetallic compounds with the $HfFe_6Ge_6$ type structure (P6/mmm, Fig. 1) are especially appropriate candidates for the study of manganese ordering by zero-field nuclear magnetic resonance (NMR) [3–11]. Most compounds order magnetically in the 400–500 K range. In dependence of the rare earth element R and temperature, various magnetic structures are realized with the individual Mn Kagomé net planes always exhibiting ferromagnetic spin arrangement. In compounds like $GdMn_6Ge_6$, all structural sites have been observed by NMR [12].

For a non-magnetic R element like lutetium, the variety of interactions is grossly reduced. Therefore pseudo-ternary intermetallic compounds like $LuMn_6Ge_{6-x}Ga_x$ ($0 \leq x \leq 1$) are an especially attractive class of compounds for the study of variations in long-range periodicity of localized Mn moments, because ferromagnetic, helical and antiferromagnetic arrangements can be realized via the Ga content, that merely acts on the Mn-Mn interlayer interactions [13–21]. The lattice constant grows in $c$ direction with Ga content $x$, and shrinks to a minor extent in $a$ direction [14–17,20]. The absolute value of the Mn moments barely varies with the Ga content $x$. The relative orientation of the moments in subsequent ferromagnetic (0 0 1) layers along the hexagonal $c$ direction is modified as follows by the Ga content [15]: $LuMn_6Ge_6$ has an antiferromagnetic structure with A-A-B-B sequence, i.e. ferromagnetic Mn-Ge(2)-Ge(3)-Ge(2)-Mn double layers and antiferromagnetic Mn-(Lu, Ge(1))-Mn arrangement (Fig. 1). According to the molecular field description of the phase diagram of antiferromagnetic $YMn_6Ge_6$, the antiferromagnetic coupling ($A_3 = -12.2$ K) is much weaker than the ferromagnetic ones ($6A_1 + A_2 = +325$ K) [22]. Thus long-distance exchange couplings ($B_1$ and $B_2$, Fig. 1c) are of decisive

[a] e-mail: edo@pi.uka.de

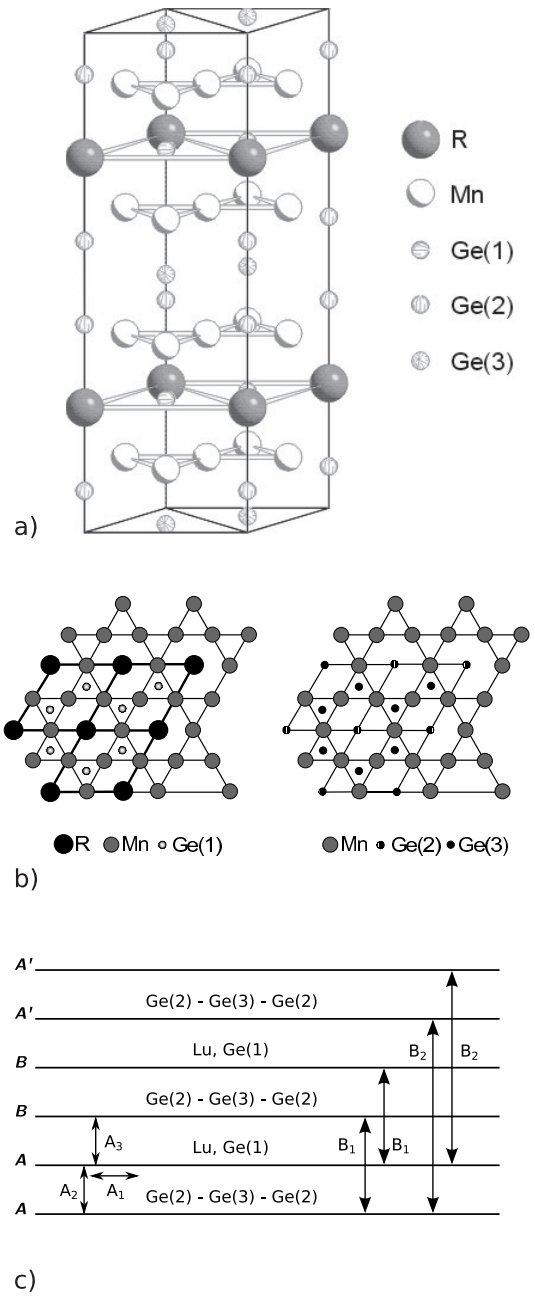


**Fig. 1.** Crystal structure of $RMn_6Ge_6$ compounds. The numbering of the Ge sites used in this contribution is defined here. It differs from [15–17], i.e. Ge(1) = Ge at (2c) site, Ge(2) = Ge at (2e) site and Ge(3) = Ge at (2d) site of the $HfFe_6Ge_6$ structure. (a) Two unit cells in $c$ direction seen perpendicular to $c$ direction. (b) Packing of Mn Kagomé nets and R, Ge layers seen along $c$-direction for Mn-(R,Ge(1))-Mn block, and Mn-Ge(2)-Ge(3)-Ge(2)-Mn block. (c) Three unit cells of $LuMn_6Ge_6$ with definition of the exchange interaction parameters within and between the manganese Kagomé net planes. The strong ferromagnetic intra- and interlayer exchange couplings $A_1$ and $A_2$ and the very weak antiferromagnetic interlayer coupling $A_3$ give rise to the A-A-B-B sequence of antiferromagnetically ordered $LuMn_6Ge_6$. The importance of the long distance coupling parameters $B_1$ and $B_2$ is responsible for the heli- and ferromagnetic structures in $LuMn_6Ge_{6-x}Ga_x$, $x = 0.4$, 0.7 and 1.0.

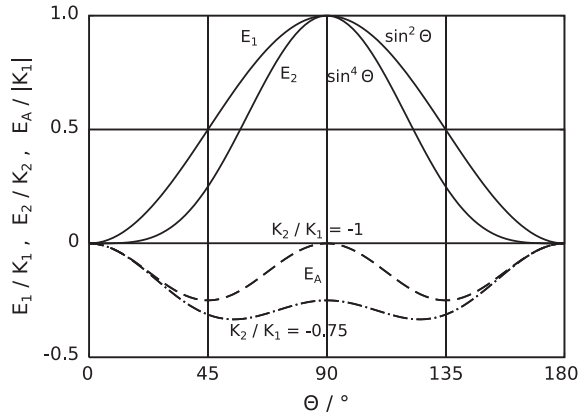


**Fig. 2.** Anisotropy energy $E_A$ and contributions $E_1$ and $E_2$ (Eq. (1)). The inclined helical structures are explained with $K_1 < 0$, $K_2 > 0$ and $|K_1| \approx |K_2|$ (broken line). A minimum of $E_A$ for $\theta = 4.8°$ or 55° results for $K_2/K_1 = -71$ (not shown) or $-0.75$ (dash-dotted line).

importance for the phase diagram, because the molecular field description predicts helical arrangements, as soon as $|B_1/(4B_2)| \leq 1$, and $B_1 = +4.84\,\mathrm{K}$ and $B_2 = -2.16\,\mathrm{K}$ were determined for $YMn_6Ge_6$ (or $+7.97\,\mathrm{K}$ and $-3.85\,\mathrm{K}$ for $DyMn_6Ge_6$) [9]. Indeed, for $LuMn_6Ge_{6-x}Ga_x$, $x = 0.4$ and (0.7), double spiral helimagnetic structures were derived at $T = 2\,\mathrm{K}$ by neutron scattering, with propagation vectors (0, 0, $q_z$) with $q_z = 0.208$ r.l.u. (0.107 r.l.u.), giving rise to large orientation differences of 66° (31°) for the Mn-(Lu, Ge(1))-Mn layer pair and small deviations of 9° (7°) between the Mn-Ge(2)-Ge(3)-Ge(2)-Mn layer pair [15]. Finally, ferromagnetic arrangement of all layers is found for $LuMn_6Ge_5Ga_1$. According to the neutron scattering data, the orientation of the manganese moments is $x$-dependent as well. Only for $x = 0$, the af ordered Mn moments seem to be aligned with the $c$ direction ($\theta = 0$), whereas for ferromagnetic arrangement at $x = 1.0$ ($\equiv x_{mp} = 0.84$ according to microprobe analysis) the inclined direction $\theta = 55°$ seemed preferred. The planes of the helical variations are inclined to the crystallographic axes, with their normal tilted by about 45° with respect to the $c$-direction. In the molecular field model description these variations are accounted for by the relative role of $K_1$ and $K_2$ in the parametrization of the anisotropy energy (Fig. 2) to be minimised [22]

$$\begin{aligned} E_A &= E_1 + E_2 \\ &= K_1 \sin^2\theta + K_2 \sin^4\theta. \end{aligned} \tag{1}$$

The preferred moment direction $\theta$, or the normal of an inclined spiral $\theta^*_\perp$, is given by [22]

$$\left.\begin{matrix} \sin^2\theta \\ \cos^2\theta^*_\perp \end{matrix}\right\} = -K_1/(2K_2). \tag{2}$$

This indicates $|K_1| \approx |K_2|$ for $x = 0.4$ and 0.7 in $LuMn_6Ge_{6-x}Ga_x$, with $K_1 < 0, K_2 > 0$. An absolute value of $K_2$ that decreases with increasing $x$ explains the observed variation in the Mn moment orientations

**Table 1.** Known low temperature magnetic data of the $LuMn_6Ge_{6-x}Ga_x$ compounds [13,15,16,18].

| $x(x_{mp})$ | $T_N/T_c/K$ | Magnetic structure | $q_z$/ r.l.u. | $\mu_{Mn}/\mu_B$ | $\theta_{Mn}$ | $\theta^*_{\perp Mn}$ | $\phi_{Mn}$ |
|---|---|---|---|---|---|---|---|
| 0 | 509, 527 | antiferromagn. | 0.5 | 2.12(7) | 0° | | – |
| 0.4(0.3) | 451 | helimagnetic | 0.2082(4) | 2.24(4) | (48°–132°) | 42(1)° | 194.4° |
| 0.7(0.55) | 372 | helimagnetic | 0.1067(6) | 2.36(5) | (45°–135°) | 45(1)° | 186° |
| 1.0(0.84) | 352 | ferromagnetic | 0 | 2.02(8) | 55.0(6)°* | | – |

$x$: nominal [15] ($x_{mp}$: microprobe analyzed [16]) composition. Moment data at $T = 2\,K$, $\theta_{Mn}$ indicates the orientation of the Mn moments with respect to the $c$ direction, $\theta^*_{\perp Mn}$ indicates the normal to the helical plane. For the double spiral helical arrangement, the phases of the Mn-R,Ge(1)-Mn layer pair (at $z \approx +1/4$ and $z \approx 3/4$–1) are shifted by $+\phi_{Mn}$ and $-\phi_{Mn}$, respectively. *Single crystal magnetization measurements indicated $\mu_{Mn} = 1.86\mu_B$ and easy-plane anisotropy, i.e. $\theta_{Mn} = 90°$, for $x_{mp} = 1.0$ [19].

**Table 2.** Data of the useful NMR isotopes in $LuMn_6Ge_{6-x}Ga_x$ [1,23].

| Isotope | Nat. abund. | $I$ | $\gamma/2\pi$/MHz/$T$ | $Q/10^{-28}$ m$^2$ |
|---|---|---|---|---|
| $^{55}$Mn | 100% | 5/2 | 10.501 | 0.330(10) |
| $^{69}$Ga | 60.2% | 3/2 | 10.248 | 0.171(2) |
| $^{71}$Ga | 39.8% | 3/2 | 13.021 | 0.107(1) |
| $^{73}$Ge | 7.6% | 9/2 | 1.490 | −0.196 |
| $^{175}$Lu | 97.4% | 7/2 | 4.863 | 3.490(20) |

in $LuMn_6Ge_{6-x}Ga_x$. Indeed, recent magnetization studies of a $LuMn_6Ge_{5.0}Ga_{1.0}$ single crystal ($x_{mp} = 1.0$) indicated easy plane anisotropy, and temperature dependent anisotropy constants with $K_1 = -0.33 MJ/m^3$ and $K_2 = +0.07\,MJ/m^3$, i.e. $K_2/K_1 = -0.21$ at 10 K. This ratio of $K_2/K_1$ results in a flattened minimum at $\theta = 90°$ in Figure 2, in contrast to $K_2/K_1 = -0.75$, with $\theta = 55°$, in the neutron scattering result of $LuMn_6Ge_{5.16}Ga_{0.84}$ [15,16,19]. Table 1 gives a synopsis of the relevant known magnetic low-temperature data of the $LuMn_6Ge_{6-x}Ga_x$ compounds.

It is worth mentioning that structural refinement with the neutron scattering data of $LuMn_6Ge_{5.0}Ga_{1.0}$ indicated a preferred but not unique occupation of the Ge(2) sites by Ga [15]. On the other hand, for the Ga-rich $ScMn_6Ge_{4.42}Ga_{1.58}$ and $ErMn_6Ge_{5.1}Ga_{0.9}$ compounds structural refinement indicated preferential occupation of the Ge(3) sites [16,17]. Our NMR analysis reported below proves indeed a substantial occupation of Ge(2) and Ge(3) sites by Ga.

In this contribution we present the results obtained from zero-field $^{175}$Lu ($I = 7/2$), $^{55}$Mn ($I = 5/2$), $^{73}$Ge ($I = 9/2$), and $^{69,71}$Ga ($I = 3/2$) NMR in $LuMn_6Ge_{6-x}Ga_x$. The interplay of magnetic hyperfine and electric quadrupolar anisotropies is explained in Section 2. Relevant experimental details are given in Section 3. Our results for the macroscopic magnetic properties (4.1) and for the Lu (4.2), Ge(4.3), Mn(4.4) and Ga nuclei (4.5) are presented in Section 4. The discussion of the results reflecting the modification of magnetic ordering by the Ga content is given in Section 5, followed by concluding remarks in Section 6.

## 2 Zero-field NMR probes in $LuMn_6Ge_{6-x}Ga_x$

All sites in $LuMn_6Ge_{6-x}Ga_x$ compounds are accessible by NMR. Table 2 collects the relevant NMR parameters. The Mn site has the lowest symmetry (2 mm). Therefore full anisotropy of the magnetic moment, of the hyperfine field and of the electric field gradient is developed. For ferrimagnetic $GdMn_6Ge_6$ with $\mu_{Mn} \approx 2.07\mu_B$ for $^{55}$Mn the three main values of the Zeeman frequency $\nu_{0,x} = 218.4\,MHz$, $\nu_{0,y} = 201.4\,MHz$, and $\nu_{0,z} = \nu_{0,c} = 241.4\,MHz$, as well as the principal value of the quadrupole splitting frequency $\Delta\nu_Q = (5.0 \pm 0.3)\,MHz$ and the asymmetry parameter of the quadrupole interaction $\eta = 0.6 \pm 0.1$ have been determined at $T = 4.2\,K$ [11]. The two latter parameters indicate that the quadrupole satellite line splitting varies between +5 MHz, −4 MHz and −1 MHz for the three main directions of quadrupolar interaction. For the less clearly resolved $^{55}$Mn-NMR spectra in the pseudo-ternary $LuMn_6Ge_{6-x}Ga_x$ compounds with non-uniform moment orientations at least the general correlation [8]

$$\nu_{0,Mn} = 108\ MHz/\mu_B \cdot \mu_{Mn} \quad (3)$$

can be used to read the manganese moment from the $^{55}$Mn NMR frequency, see Section 4.4.

For all other sites in $LuMn_6Ge_6$, the symmetry is higher and the $c$ axis is the principal axis of the axial site symmetry. Thus anisotropy of the magnetic hyperfine interaction is reduced to

$$\nu(\theta) = \nu_{is} + \nu_{an}(3\cos^2\theta - 1)/2 \quad (4)$$

and quadrupolar interaction is described by $\Delta\nu_Q \neq 0$, but $\eta = 0$. Figure 3 shows the typical variation of the NMR spectrum with angle $\theta$ that can be predicted for the $^{73}$Ge ($I = 9/2$) nucleus with parameters appropriate for the Ge(2) site ($\nu_{is} = 11\,MHz$, $\nu_{an} = 3\,MHz$, $\Delta\nu_Q = 1\,MHz$, exact diagonalization, individual half width at half height (HWHH) 50 kHz).

The three Ge sites in $LuMn_6Ge_{6-x}Ga_x$ (Fig. 1) can not be distinguished by qualitative features of the respective NMR spectra. Therefore the electric field gradients at these sites were calculated with the WIEN2k program package for $LuMn_6Ge_6$ [24,25]. The respective quadrupolar splitting parameters $\Delta\nu_Q$ are reported in Table 3. Comparison with the experimental data for $GdMn_6Ge_6$

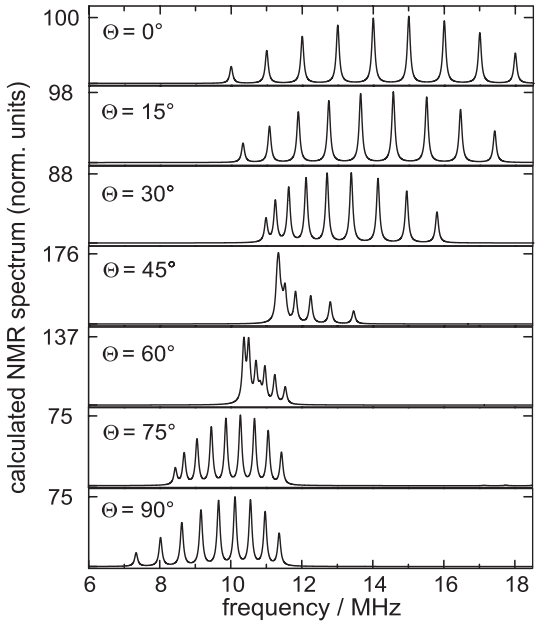


**Fig. 3.** Variation of the $^{73}$Ge ($I = 9/2$) NMR spectrum with the angle $\theta$ of the local field with respect to the crystallographic $c$ direction for parameters typical for the Ge(2) site ($\nu_{is}$ = 11 MHz, $\nu_{an}$ = 3 MHz, $\Delta\nu_Q$ = 1 MHz, $T$ = 4.2 K) calculated by exact diagonalization, adopting a half width at half height (HWHH) of 50 kHz, normalized to 100 for the maximum of the $\theta = 0°$-spectrum.

**Table 3.** NMR parameters of $^{73}$Ge at the Ge sites in $LuMn_6Ge_{6-x}Ga_x$ and $GdMn_6Ge_6$ (Fig. 1).

| | Ge(1) | Ge(2) | Ge(3) |
|---|---|---|---|
| $LuMn_6Ge_6$ | | | |
| calc. $\Delta\nu_Q$/MHz | 2.069 | 0.941 | 2.733 |
| exp. $\Delta\nu_Q$/MHz | – | 0.97(2) | 3.20(2) |
| $\nu_{0,\parallel c} = \nu_{is} + \nu_{an}$/MHz | – | 11.20(2) | 28.80(2) |
| $GdMn_6Ge_6$ [3] | | | |
| $\Delta\nu_Q$/MHz | 2.10(1) | 1.14(2) | 3.22(3) |
| $\nu_{0,\perp c} = \nu_{is}$-$\nu_{an}/2$/MHz | 19.68(2) | 7.80(1) | 25.04(4) |
| $LuMn_6Ge_{6-x}Ga_x$ | | | |
| $x = 0.4$ | | | |
| $\Delta\nu_Q$/MHz | 2.1(1) | 1.00(3) | 3.29(4) |
| $\nu_{is}$/MHz | 14.59(15) | 10.88(8) | 25.26(8) |
| $\nu_{an}$/MHz | −9.22(15) | 2.72(8) | 0.18(4) |
| $x = 0.7$ | | | |
| $\Delta\nu_Q$/MHz | 2.2(1) | 1.00(3) | 3.27(4) |
| $\nu_{is}$/MHz | 15.89(15) | 10.72(8) | 24.62(8) |
| $\nu_{an}$/MHz | −10.22(15) | 2.68(8) | 0.17(4) |
| $x = 1.0$ | | | |
| $\Delta\nu_Q$/MHz | 1.9(1) | 0.95(3) | 3.19(7) |
| $\nu_{is}$/MHz | 14.59(15) | 11.12(8) | 23.77(17) |
| $\nu_{an}$/MHz | −9.22(15) | 2.78(8) | 0.17(8) |

For $GdMn_6Ge_6$, the assignment of the NMR spectra to the crystallographic sites Ge(2) and Ge(3) had to be interchanged with respect to reference [3] on account of the calculated electric field gradients.

shows that a unique site assignment is achieved [3]. The assignment of sites Ge(2) and Ge(3) had to be interchanged with respect to the earlier published one. The assignment in Table 3 explains now easily the early NMR observations in $Gd_xY_{1-x}Mn_6Ge_6$ for $x$ decreasing from $x = 1$ [5,22]. The $^{73}$Ge spectrum of the Ge(3) sites, most distant from the Gd/Y site, remained constant down to the lowest concentration $x = 0.5$, whereas that of the Ge(1) site residing in the R = Gd/Y plane could only be observed for $x = 1.0$, 0.9 and 0.8.

NMR in magnetically ordered materials with spontaneous macroscopic magnetization gives rise to domain and wall signals, and enhancement of radiofrequency fields as well as NMR signals [1]. These peculiarities have to be considered in the following discussions especially for the nominally $x = 1.0$ compound. For this compound, the NMR spectra depend on the excitation conditions. For small radiofrequency (rf) power, only wall signals are observed, with $\theta$ varying between 55° and 125° and maximum enhancement for $\theta = 90°$ (Tab. 1). On the other hand, for high rf power, the wall edge and domain signals predominate clearly ($\theta \approx 55°$) due to the larger number of spins residing in domains than in walls. For the helimagnetic structures ($x = 0.4, 0.7$), the homogeneous distribution of Mn spin directions rotating in planes inclined with respect to the $c$ symmetry axis yields a non-uniform distribution of $\theta$-values, as exemplified in the upper part of Figure 4. The $\theta$-dependence of hyperfine field (Eq. (4)) and quadrupolar splitting visualized e.g. for the Ge(2) site in Figure 3 has to be folded with this $\theta$-probability distribution. Thus the two orientations $\theta = 90°$ and $\theta_{min}/\theta_{max}$ stand out in the spectra of $^{73}$Ge and $^{69,71}$Ga as shown in the lower part of Figure 4, and the $\theta_{min}$ and $\theta_{max}$ signatures predominate in the spectra.

Due to the large electric field gradient at the R-site of $RMn_6Ge_6$ compounds [6,7] and the – in this respect – rather unfavourable NMR parameters of the predominant isotope $^{175}$Lu (Tab. 2), it is more complicated to use this isotope as a NMR probe in the helimagnetic $LuMn_6Ge_{6-x}Ga_x$ compounds. For the antiferromagnetically ordered $LuMn_6Ge_6$ compound four nuclear quadrupole resonance (NQR) transitions of $^{175}$Lu can be clearly resolved, however (Sect. 4.2), and prove an earlier suggested double cone distortion of the antiferromagnetic arrangement.

## 3 Experimental

Sample preparation was described in references [14,15,18,20]. The purity of the samples was checked by powder X-ray diffraction. Only very weak lines belonging to the $Lu_2O_3$ oxide were observed. Magnetic moment and susceptibility were determined for powdered samples with a Quantum Design superconducting quantum interference device (SQUID) magnetometer, see Figure 5. The powder samples were enclosed in glass crucibles of 4 mm inner/6 mm outer diameter for the NMR experiments. The $^{73}$Ge NMR spectra and the

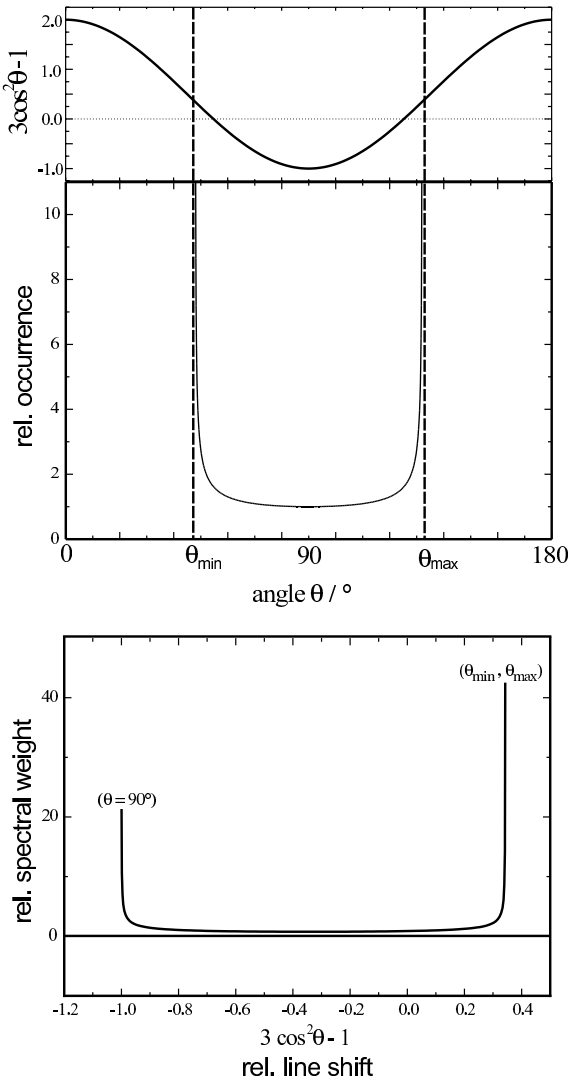


**Fig. 4.** Angular dependence of anisotropic NMR contributions and weighting factor for the respective $\theta$ values versus angle $\theta$ with axial $c$ direction for helimagnetic structures. $\theta^*_{\perp \mathrm{Mn}} = 42°$, appropriate for $LuMn_6Ge_{5.6}Ga_{0.4}$, is used (Tab.1). Folding of the two upper dependences gives the lower spectral weight distribution. It visualizes that $\theta = 90°$ and $\theta = \theta_{min}, \theta_{max}$ yield the most pronounced spectral features, occurring for $3\cos^2\theta - 1 = -1$ and $3\cos^2\theta_{min/max} - 1 = +0.343$.

$^{175}$Lu NQR spectrum at frequencies below 50 MHz were recorded with a Bruker MSL 300 spectrometer with tuned home built probehead, using Fourier transforms of the second half of the spin echo, excited by two pulses of 1 and 2 $\mu$s length and 40 $\mu$s separation (Figs. 6–8). Temperature was controlled with help of an Oxford Instruments CF 1200 He gas flow cryostat. Only data for $T = 4.2$ K are presented. In Figures 7 and 8, the section of the Fourier transforms within the excitation width for varied excitation frequencies is plotted directly versus frequency, dubbed "FT amplitude", whereas in all other cases the integral over the excitation width is plotted as "NMR signal". The sharpness of the "lines" visible in Figures 7 and 8, which is influenced by the excitation spectrum, should thus not be mixed-up with the real sharpness of the spectral features plotted in Figures 6 for pure $LuMn_6Ge_6$ (exhibited in spite of the forgoing spectral integration). Usually, NMR signals grow with the square of the frequency: one linear-in-frequency dependence results from the induction law, the other one from the difference in thermal population of the nuclear levels. Since the latter factor is considered also in the simulated spectra (see e.g. Fig. 3), only the former linear-in-frequency dependence was corrected in Figures 7 and 8. NMR signals in the 50–450 MHz range were recorded with a home built broad band system based on the Bruker MSL 300 spectrometer ($\leq$125 MHz) or a Tecmag APOLLO NMR console, with non-resonant, uncalibrated probehead. Measuring temperature $T = 4.2$ K was achieved by inserting the probehead directly in a liquid Helium storage vessel. Again Fourier transforms of the second half of the spin echo excited now by two pulses of 1 and 2 $\mu$s length and 30 $\mu$s separation, were calculated and integrated over $\pm$0.25 MHz around the excitation frequency. This quantity is plotted as NMR signal, and was analysed in dependence of the radiofrequency power and pulse separation for a detailed characterization of the origin of the respective signals (Figs. 9–11).

## 4 Results

### 4.1 Macroscopic magnetic properties

The magnetization data of the powder samples studied here confirm the ferromagnetic ordering of $LuMn_6Ge_5Ga_1$ [15], with a field dependent transition temperature $T_c = 335$–$365$ K, see Figure 5g. On the other hand, the susceptibility in the antiferromagnet $LuMn_6Ge_6$ ($T_N \approx 500$ K) varies with temperature, as was concluded earlier [21]. The low-temperature anomalous increase visible in Figures 5a, 5b may be related to the formation of a small-angle double-cone structure [13], but could also be explained by the contribution of a paramagnetic impurity [18]. The characteristic NQR/NMR-spectrum of $^{175}$Lu observed for this compound at 4.2 K proves unambiguously the non-collinear arrangement of the manganese moments, however (Sect. 4.2). For the intermediate compositions, antiferromagnetic ordering ($T_N \approx$ 430 (350) K) for $x = 0.4$ (0.7) is confirmed, as well as the transition to a helimagnetic arrangement below room temperature for $x = 0.4$ or at $T_N$ for $x = 0.7$ [15]. The insets to Figures 5f and 5g reveal that the deviation from field-independence of the magnetic susceptibility sets in at higher temperatures than the tabulated $T_N/T_c$ - values of Table 1, already. The respective characteristic temperatures, i.e. 435 (495) K for $x = 0.7$ (1.0), fall close to the $T_N$-values of the $x = 0.4$ (0) compounds. These results indicate that in all four compounds correlations and short range or long range antiferromagnetic order starts at 430–500 K already. Subsequently, at 350 K or below, transition to canted antiferromagnetic, helical or ferromagnetic arrangement takes place. The NMR analysis is restricted to the low-temperature range (4.2 K)

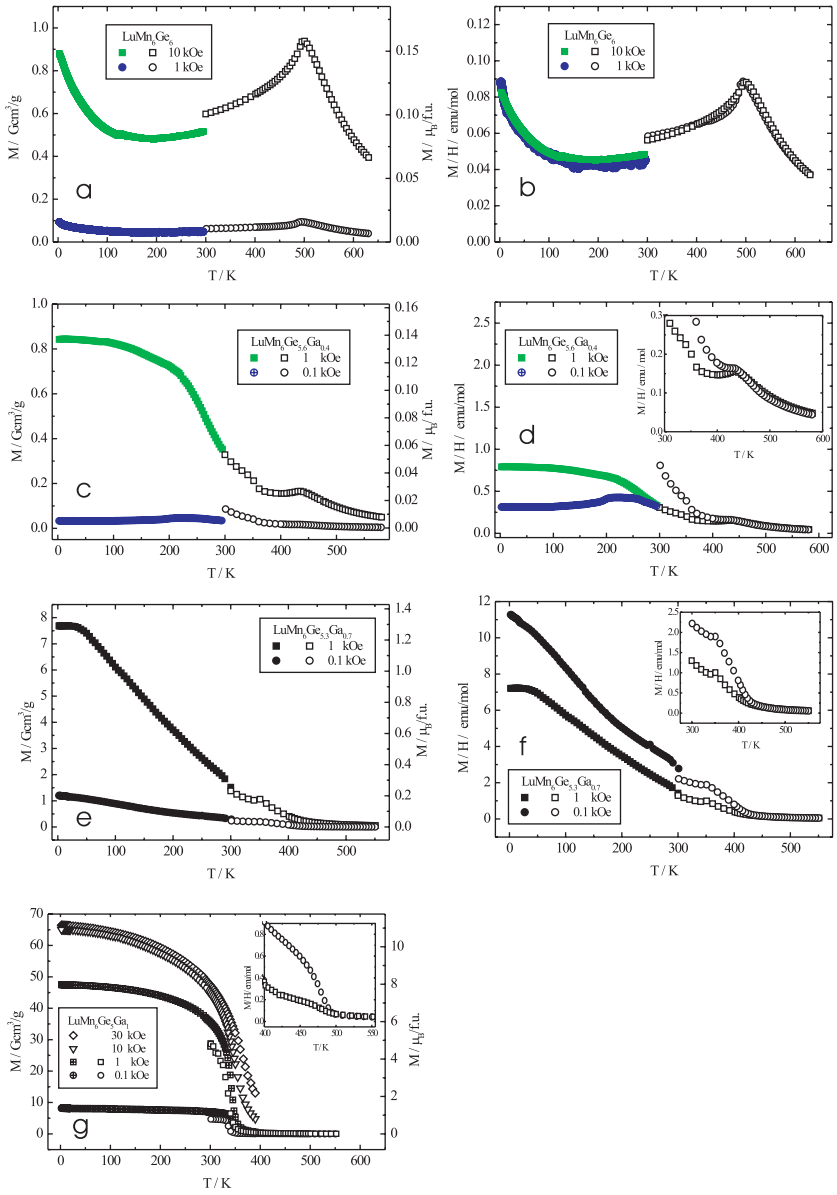


**Fig. 5.** (Color online) Temperature and magnetic field dependence of magnetic moments per gram or formula unit ($\mu_B$/f.u.) in (a), (c), (e), and (g), and molar susceptibilities ($M/H$) in (b), (d), (f), and (g) of the four $LuMn_6Ge_{6-x}Ga_x$ powder samples with $x = 0$, 0.4, 0.7, and 1.0 studied by NMR in this investigation. Low- and high-temperature ranges were measured with different inserts of the SQUID magnetometer, the low-temperature data in (a)–(d) with a different sample portion and a vibrating sample magnetometer. Therefore these data are distinguished in the figures.

allowing the comparison of antiferromagnetic, helimagnetic and ferromagnetic arrangement for $x$ growing from $x = 0$ to $x = 1$ in $LuMn_6Ge_{6-x}Ga_x$.

### 4.2 Lutetium NQR

Several frequency ranges of the NMR spectra in $LuMn_6Ge_{6-x}Ga_x$ can be distinguished. In the low-frequency range 5–40 MHz, the multi-line spectra of $^{73}$Ge with nuclear spin $I = 9/2$ predominate. Figure 6 shows an especially simple case, because only two of the three Ge sites contribute to $^{73}$Ge NMR. In the frequency range 200–240 MHz, the $^{55}$Mn signals are observed (Fig. 9a). The $^{69}$Ga and $^{71}$Ga signals span an extremely broad range from about 70–340 MHz. For most sample compositions, the $^{175}$Lu NMR signals are hidden under the $^{73}$Ge and $^{69,71}$Ga signals due to their wide frequency spread. For the antiferromagnetic ($x = 0$) compound $LuMn_6Ge_6$, the A-A-B-B sequence of the magnetically ordered manganese double layers grants in case of collinear arrangement the exact compensation of the transferred magnetic hyperfine interaction at the Lu site. Thus a pure NQR spectrum would have to be observed, with three lines at $1 \times \Delta\nu_Q, 2 \times \Delta\nu_Q$ and $3 \times \Delta\nu_Q$ for the $\pm 1/2 \leftrightarrow \pm 3/2, \pm 3/2 \leftrightarrow \pm 5/2$ and $\pm 5/2 \leftrightarrow \pm 7/2$ transitions, respectively. Using the WIEN2k program package, $^{175}\Delta\nu_Q = 21.4$ MHz was calculated for $LuMn_6Ge_6$ [24,25]. Converting the observed $\Delta\nu_Q$-values of $^{155,157}$Gd in $GdMn_6Ge_6$ [7] to the nuclear parameters of $^{175}$Lu suggests $\Delta\nu_Q \approx 18.5$ MHz, rather close to the actually observed value for the upper two NQR resonances at $\approx 2 \times \Delta\nu_Q$ and $\approx 3 \times \Delta\nu_Q$ indicated in Figure 6. The NQR/NMR-spectrum of $^{175}$Lu shows, however, unequivocally that the lowest frequency transition is split considerably, whereas the line at 48.6 MHz is not (Fig. 6). This results from a small magnetic field (Zeeman)

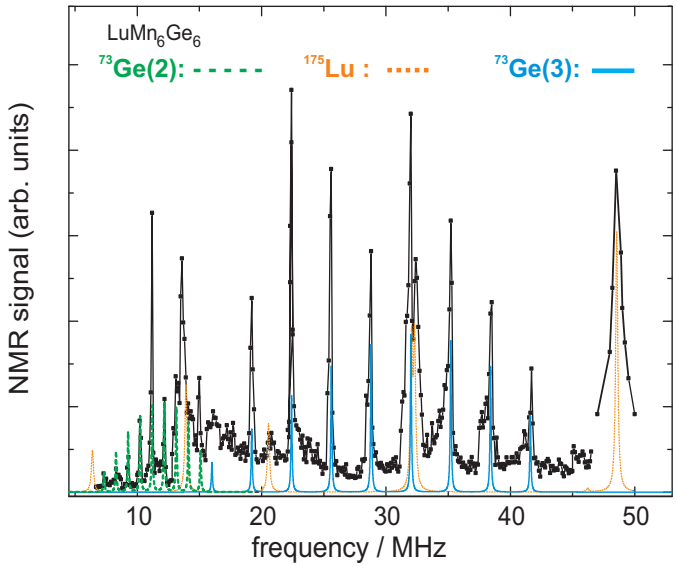


**Fig. 6.** (Color online) NMR and NQR spectrum of $LuMn_6Ge_6$ at 4.2 K in the low-frequency range as well as calculated spectra (solid and broken (colored) lines, HWHH = 50 kHz). The NMR transitions of $^{73}$Ge(2) (green) and $^{73}$Ge(3) (blue) as well as four out of five NQR/NMR transitions of $^{175}$Lu (orange) can be distinguished. For the parameters see Section 4.2 and 4.3.

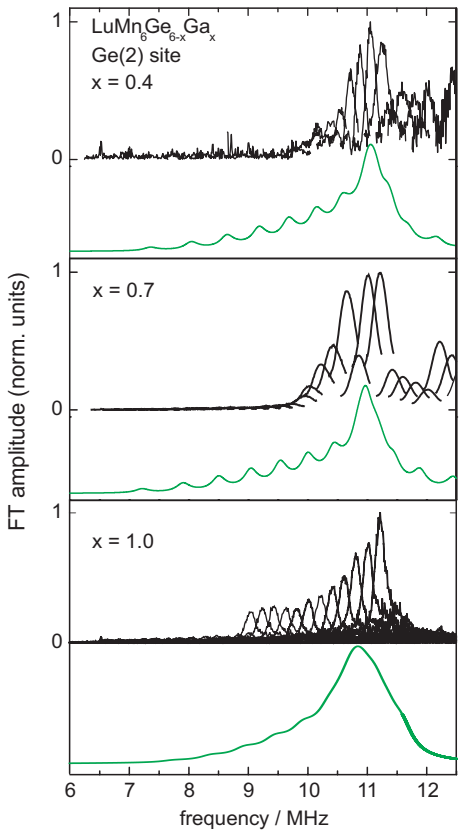


**Fig. 7.** (Color online) $^{73}$Ge zero-field NMR spectra (FT amplitudes) of $LuMn_6Ge_{6-x}Ga_x$ for $x = 0.4, 0.7$ and 1.0 at $T = 4.2$ K (range of the Ge(2) site signals). The signals are non-zero beginning from the low-frequency end of the trace and are divided by the frequency in order to correct for the frequency dependence of the induction law and to improve comparability with the calculated spectra within the broad frequency range. The solid (green) lines show the fits explained in the text (Section 4.3) (HWHH = 100 kHz (200 kHz) for $x = 0.4$ and 0.7 (1.0)). The fit parameters are collected in Table 3.

contribution that must be oriented perpendicular to the $c$-direction, the orientation of the predominating electric field gradient. Otherwise, all transitions would be influenced by the component of the magnetic field that is oriented parallel to the predominating field gradient's direction $c$ [26]. The resulting complicated splitting pattern was derived by exact diagonalization. $^{175}\Delta\nu_Q = (16.20 \pm 0.05)$ MHz, and $^{175}\nu_0(90°) = 1.66$ MHz is derived for $LuMn_6Ge_6$ at $T = 4.2$ K. The latter value can be compared to its maximum value of $^{175}\nu_M(90°) = 19.75$ MHz, calculated from the results of the detailed analysis of $GdMn_6Ge_6$ [7]. (The ferrimagnetic order of $GdMn_6Ge_6$ comes along with parallel orientation of all Mn magnetic moments of the various planes. The magnetic hyperfine field transferred from Mn to the Gd nuclei has been separated (+33 kOe) [7], and is converted to $^{175}\nu_M(90°)$ by considering the 23% larger hyperfine coupling constant of $^{175}$Lu [1] and the respective nuclear data (Tab. 2).) The ratio 1.66/19.75 indicates that the deviation from collinear antiferromagnetic structure with moments oriented parallel to the $c$-axis is small and a cone angle of about 4.8° is sufficient to explain the observed transversal field within a double cone magnetic phase of $LuMn_6Ge_6$.

### 4.3 Germanium NMR

Assuming that primarily the nearest neighbour Mn-layers are responsible for the hyperfine field at the Ge sites, for the Ge(1) sites (Figs. 1a and 1b) a characteristic dependence of the Zeeman frequency on the $q_z$-value (Tab. 1) according to

$$\nu_0(x) \approx \nu_0(x = 1) \cdot \cos(\pi q_z \cdot 0.5\text{l.u.} + \phi_{\mathrm{Mn}}) \qquad (5)$$

is predicted (neglecting the anisotropy, Eq. (4)). According to this relation a ratio of 0:0.84:0.96:1 for the respective Ge(1) resonance frequencies for the $x = 0$, 0.4, 0.7 and 1.0 compounds is expected for $LuMn_6Ge_{6-x}Ga_x$ neglecting variations of the Mn moment with $x$ and the small double cone angle for $x = 0$ (yielding the finite value 0.08 instead of 0). In agreement with this argument, no $^{73}$Ge(1) signal is observed for $x = 0$ in Figure 6. This supports the site assignment based on the calculated quadrupolar interaction (Tab. 3). Because $\theta_{\mathrm{Mn}} \approx 0$ for $x = 0$, equidistant quadrupolar satellite lines are predicted and observed according to [27]

$$\nu(m \to m-1) = \nu_0 \pm \frac{\Delta\nu_Q}{2}(m - \frac{1}{2})(3\cos^2\theta - 1) + \frac{\Delta\nu_Q^2}{32\nu_0}(1 - \cos^2\theta)\left[\{102m(m-1) - 406.5\}\cos^2\theta - \{6m(m-1) - 46.5\}\right] \qquad (6)$$

with $\Delta\nu_Q = | eQV_{zz}/24h |$ for $I = 9/2$. Figure 6 shows the $^{73}$Ge spectra recorded at $T = 4.2$ K as well as the

calculated resonance line positions. Perfect agreement is obtained. The NMR-parameters are given in Table 3. The small wings of the NMR lines visible e.g. at 24 MHz and 34 MHz for the Ge(3) site in Figure 6 reflect the small deviations from $c$-axis oriented collinear Mn moment arrangement deduced from the $^{175}$Lu-NQR/NMR spectrum above.

A comparison between the data of $LuMn_6Ge_6$ ($\theta \approx 0°$, $c \approx 8.13$ Å) and $GdMn_6Ge_6$ ($\theta = 90°$, $c \approx 8.18$ Å) is enlightening (Tab. 3). Evidently, the variation of the quadrupole splitting parameters $\Delta\nu_Q(2)$ and $\Delta\nu_Q(3)$ is negligible. On the other hand, the comparison points to a pronounced anisotropy of the magnetic hyperfine interaction, with $\nu_{an}/\nu_{is}$ amounting to about 25% for the Ge(2) site and about 10% for the Ge(3) site. This is reflected by the large width and smeared line splittings in the $^{73}$Ge spectra for $x \neq 0$ for the Ge(2) site in Figure 7 and for the Ge(1) but not the Ge(3) sites in Figure 8. For the helimagnetic structures in $LuMn_6Ge_{6-x}Ga_x$ with $x = 0.4$ and 0.7, the solid line fits take the angular dependence of the weight factor (Fig. 4) and of the line positions along equations (4) and (6) (using, however, exact diagonalization, see Fig. 3) into account. For the ferromagnetic compound with $x = 1.0$, depending on excitation conditions either domain and wall edge ($\theta = 55°$) or wall signals ($55° < \theta < 125°$) could be excited (Fig. 8b). The respective angular weight factors, differing then from Figure 4, were taken into account for the $x = 1.0$ line fits [28]. The low resolution of the Ge(1) and Ge(2) site spectra in Figures 7 and 8 is a support of a domain $\theta$ value of $55° < 90°$ for the $x = 1.0$ ($x_{mp} = 0.84$) sample (Tab. 1), because easy plane ($\theta = 90°$) spectra, that would result for $x_{mp} = 1.0$ according to single crystal magnetization data [19] would be well resolved, as was shown earlier for the $GdMn_6Ge_6$ compound [3,12]. The quantitative description of all $^{73}$Ge NMR spectra in $LuMn_6Ge_{6-x}Ga_x$ for $0 \leq x \leq 1$ was thus accomplished successfully. All fit parameters are collected in Table 3.

### 4.4 Manganese NMR

The $^{55}$Mn NMR spectrum of antiferromagnetic $LuMn_6Ge_6$ at $T = 4.2$ K was reported before (1.5 $\mu$s-15 $\mu$s-3 $\mu$s-spin echo sequence) [22]. The maximum of the spectrum was observed at $\nu_{0,c} = 231.2$ MHz, that means 10 MHz lower than the $c$-axis value of $GdMn_6Ge_6$. The Mn moment of $\mu_{Mn} \approx 2.14\,\mu_B$ deduced via equation (3) is in agreement with the value indicated in Table 1. The $^{55}$Mn NMR spectra recorded for $x = 0.4$, 0.7, and 1.0 are presented in Figure 9a. The typical dependence of these signals on the radiofrequency power is shown in Figure 9b. Both diagrams show a monotonous variation with the Ga content $x$. Let us start with the enhancement factor (Fig. 9b): the highest power is required for the $x = 0.4$ sample of $LuMn_6Ge_{6-x}Ga_x$, that resembles in this respect most to the antiferromagnetic $x = 0$ compound. The broad maximum starting at very low power observed for $x = 1.0$ is typical for ferromagnetic materials with wall-center and wall-edge contributions.

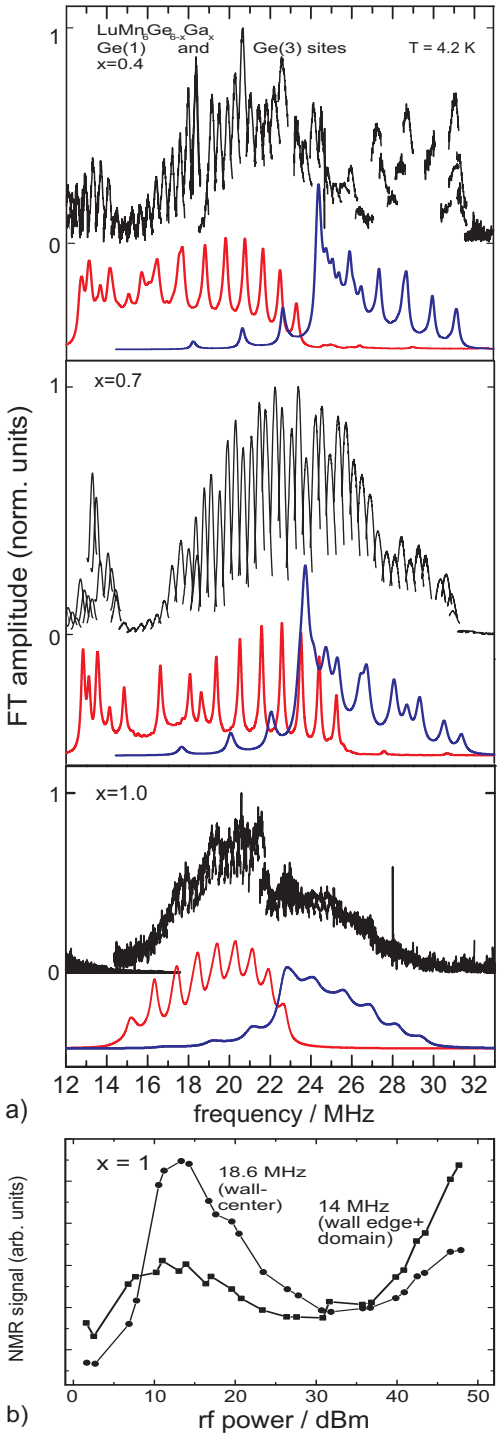


**Fig. 8.** (Color online) (a) $^{73}$Ge zero-field NMR spectra (FT amplitude) of $LuMn_6Ge_{6-x}Ga_x$ for $x = 0.4, 0.7$ and 1.0 at $T = 4.2$ K (range of the Ge(1) and Ge(3) signals). The signals are divided by the frequency (see Fig. 7). The solid lines show the fit explained in the text (Section 4.3). (HWHH = 200 kHz; Ge(1), red line, lower frequencies; Ge(3), blue line, higher frequencies.) The smaller ratio of $\nu_{an}/\nu_{is}$ explains that quadrupolar split lines are resolved only for the Ge(3) site (for $x = 0.4$ and 0.7). The fit parameters are collected in Table 3. (b) Dependence of the signal strength on radio-frequency power for the low- (squares) and high-frequency (points) range of the Ge(1) site spectrum for the ferromagnetic sample $x = 1.0$.

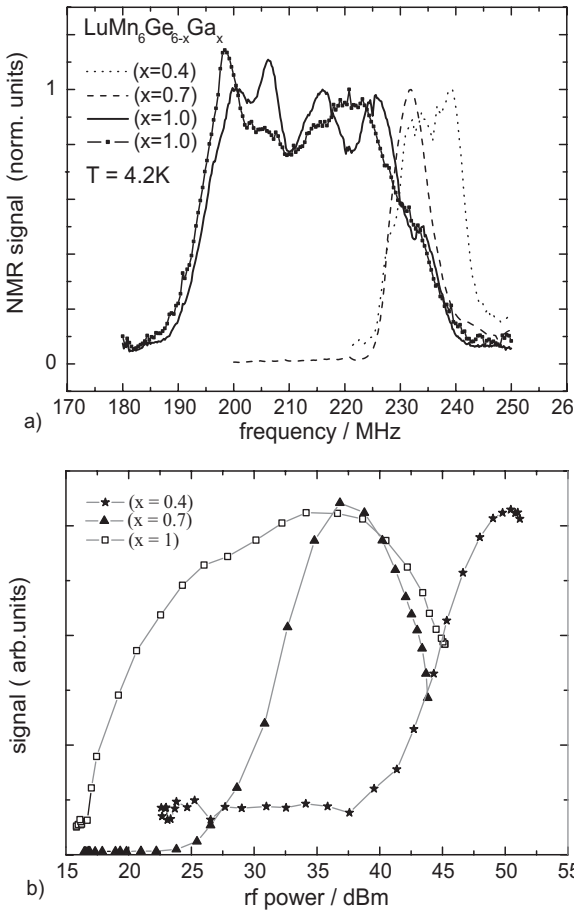


**Fig. 9.** $^{55}$Mn zero-field NMR spectra of $LuMn_6Ge_{6-x}Ga_x$ for $x = 0.4, 0.7$ and 1.0 at $T = 4.2$ K (a), and dependence of the respective signal strength on radio-frequency power (b). For $x = 1.0$ two different spectra recorded with different excitation conditions are shown. The $x = 1.0$ $^{55}$Mn spectrum is superimposed by $^{69}$Ga(3) signals at the high frequency wing (Fig. 11), and $^{71}$Ga(1) signals at frequencies below 210 MHz. For discussion see Section 4.4.

The latter's higher power requirement agrees with that of the $x = 0.7$ helimagnetic compound. The center frequency of the $^{55}$Mn spectra shifts systematically with growing $x$ to lower frequencies (Fig. 9a). From the center frequencies 236(4) MHz, 232(1) MHz and 221(5) MHz, we deduce with equation (3) Mn moments of $2.19(4)\mu_B, 2.15(1)\mu_B$ and $2.05(4)\mu_B$ for $x = 0.4, 0.7$ and 1.0, respectively. The agreement with the neutron scattering results reproduced in Table 1 is persuasive, taking into account that deviations by up to 9.5% might be caused by anisotropic orbital contributions, as alluded to in Section 2 (for $GdMn_6Ge_6$).

On a first glance, the variation of the width and line structures with $x$ in Figure 9a is peculiar. We mentioned in Section 2 that the $^{55}$Mn quadrupole satellite line separation varies between $\Delta\nu_Q = +5$ MHz and $-4$ MHz for Mn moment in the Kagomé net plane and $-1$ MHz along the $c$ direction for $GdMn_6Ge_6$. Our calculation for the Mn site based on the WIEN2k program package gave the three main values $\Delta\nu_{Q,i}$ of the quadrupolar splitting frequency $+1.69$ MHz, $-1.60$ MHz and $-0.09$ MHz for paramagnetic $LuMn_6Ge_6$ [24,25]. Thus average splittings of $|\,\Delta\nu_Q\,| = 3.6$ MHz and 2 MHz deduced from the width of the $^{55}$Mn spectra for $x = 0.4$ and 0.7 are in line with these values and the helimagnetic variation of the moment orientation. On the other hand, the apparently resolved splitting of $\Delta\nu_Q = 8.4 \pm 1.8$ MHz of $LuMn_6Ge_5Ga_1$ is clearly outside this range of values. We will show in Section 4.5, however, that the broad "Mn"-NMR spectrum of $LuMn_6Ge_5Ga_1$ shown in Figure 9a can be explained by the overlap of three different spectral features — three lines of $^{71}$Ga at Ge(1) sites at the low frequency side, three lines of $^{69}$Ga at Ge(3) sites at the high frequency side, and only the central part due to $^{55}$Mn. Nevertheless, a larger error of the NMR estimate of the Mn moment has to be conceded for the $x = 1.0$ composition.

### 4.5 Gallium NMR

There exists no previous report of $^{69,71}$Ga NMR spectra in $RMn_6Ge_{6-x}Ga_x$ compounds. Therefore it is helpful for the identification of the NMR signals to relate the expected $^{69,71}$Ga Zeeman frequencies and quadrupolar splittings to the known $^{73}$Ge spectral parameters (Tab. 3). Neglecting the reduction of the outer electron number by one, when Ge is replaced by Ga, but in compliance with the much larger gyromagnetic ratio (Tab. 2), and the comparable outer electron hyperfine coupling constants $A_{4s}$ [1], an about 5.4 (or 6.9) times higher resonance frequency is expected for $^{69}$Ga (or $^{71}$Ga) than for $^{73}$Ge according to $^{69(71)}\nu_0 = {}^{73}\nu_0 \cdot (^{69(71)}\gamma/^{73}\gamma) \cdot (A_{4s}(\mathrm{Ga})/A_{4s}(\mathrm{Ge}))$ with $A_{4s}(\mathrm{Ga}) = 4.5$ MOe/spin, $A_{4s}(\mathrm{Ge}) = 5.7$ MOe/spin. On the other hand, due to the smaller nuclear spin, but comparable quadrupole moment, by a factor of about 10.5 (or 6.6) larger quadrupole splitting frequencies $\Delta\nu_Q$ are predicted for the Ga isotopes assuming unvaried electric field gradients, i.e. $^{69(71)}\Delta\nu_Q = {}^{73}\Delta\nu_Q \cdot 12 \cdot (^{69(71)}Q/^{73}Q)$.

According to neutron structural refinement, the Ge(2) site (Figs. 1a and 1b) is preferred for Ga occupation in $LuMn_6Ge_{6-x}Ga_x$ [15]. The respective observed $^{69}$Ga and $^{71}$Ga NMR spectra together with the corresponding simulated spectra are shown in Figure 10. The fit parameters are compiled in Table 4. The parameter ratios of the two isotopes agree with the tabulated values (Tab. 2) within the typical accuracy of some percent. The observed NMR-parameters show that our estimated scaling factors were quite useful: the quadrupolar splitting frequencies for $^{69(71)}$Ga are indeed 9.0–9.5 (or 6.0–6.3) times larger than for $^{73}$Ge (this means, only about 10% smaller than estimated). The reduced outer electron number of Ga gives rise to a 50% increased hyperfine field, however, because the ratio of the $^{69}$Ga (or $^{71}$Ga) and $^{73}$Ge Zeeman frequencies is 8.3 (or 10.2–10.5), which is 50% larger than the converted values of the Ge(2) site.

The $^{69,71}$Ga NMR spectra for the highest frequency range originating from Ga at the Ge(3) site are shown in Figure 11. This site seemed preferred in $ScMn_6Ge_{4.42}Ga_{1.58}$ and $ErMn_6Ge_{5.1}Ga_{0.9}$ [16,17] and the

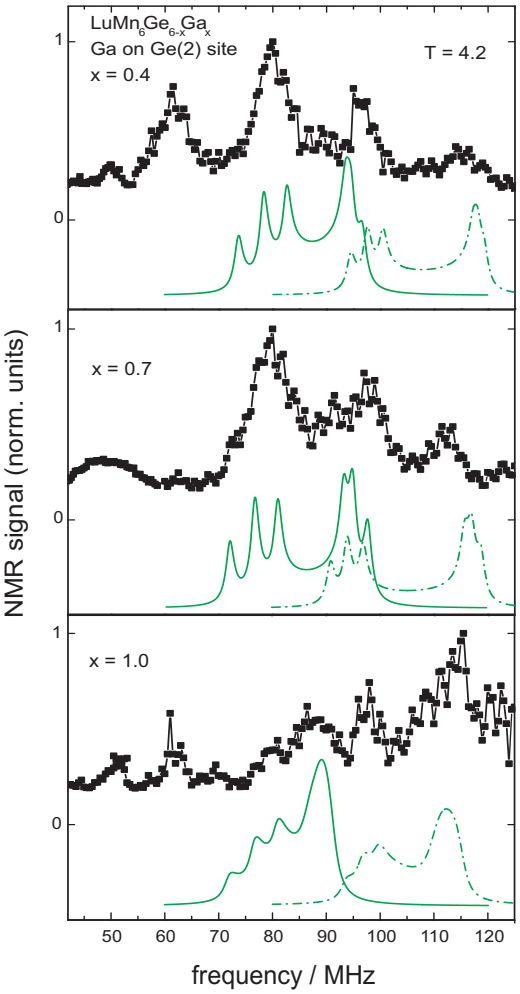


**Fig. 10.** (Color online) $^{69}$Ga and $^{71}$Ga zero-field NMR spectra of $LuMn_6Ge_{6-x}Ga_x$ for $x = 0.4$, 0.7 and 1.0 at $T = 4.2$ K for Ga on the Ge(2) site, together with the corresponding simulated spectra. ($^{69}$Ga: solid (green) line, HWHH = 0.9 MHz, $^{71}$Ga: dash-dotted (green) line, HWHH = 1.1 MHz. For parameters see Tab. 4). In the low frequency part, signals of $^{175}$Lu can be seen [28].

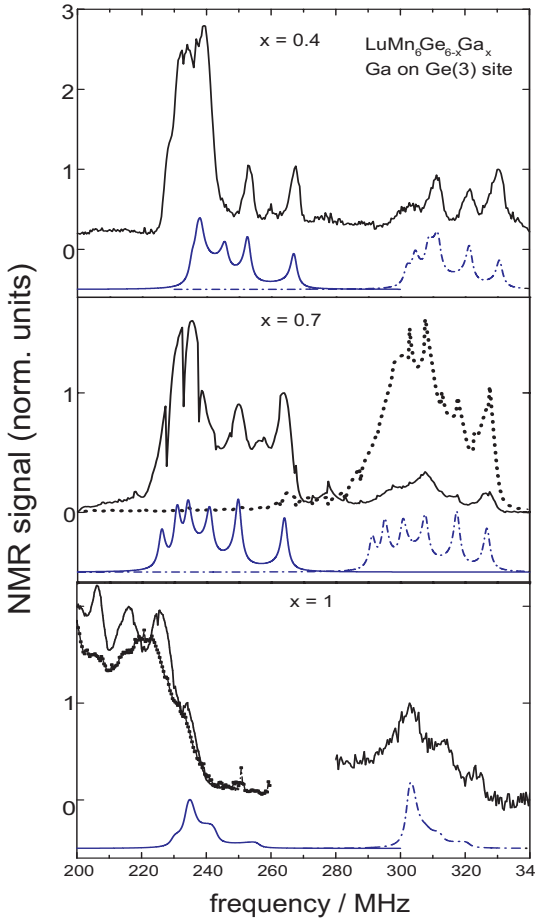


**Fig. 11.** (Color online) High-frequency $^{69,71}$Ga zero-field NMR spectra of $LuMn_6Ge_{6-x}Ga_x$ for $x = 0.4, 0.7$ and 1.0 originating from Ga on Ge(3) sites at $T = 4.2$ K for optimized radiofrequency power (two different excitation conditions for $x = 0.7$ and 1.0). In the 220–240 MHz range, $^{55}$Mn signals predominate. Above 280 MHz, the $^{71}$Ga signals (dash-dotted (blue) line fit) and below 270 MHz the $^{69}$Ga signals (solid (blue) line fit) are observed. HWHH = 1.1 MHz. (Regular anomalies of the spectra at $(n \cdot 10 \pm 2.5)$ MHz are due to power variation of the transmitter.) The fit parameters are compiled in Table 4.

Ga NMR signal strength visible in Figure 11 supports relevant occupation of this site also for $LuMn_6Ge_{6-x}Ga_x$. These spectra can easily be assigned to Ga based on the ratio of the nuclear data of the two isotopes $^{69}$Ga (lower frequencies) and $^{71}$Ga (higher frequencies) (Tab. 2). Splitting into three lines can clearly be seen for the line group around 300–330 MHz for $x = 0.4$ and 1.0 (Fig. 11). These well resolved $^{71}$Ga lines can be used to assign the lower frequency $^{69}$Ga lines overlapping partially with $^{55}$Mn signals, and to unravel the $x$-dependence of these spectra. The parameters derived for $^{69,71}$Ga(3) by the line profile simulation based on Section 2 are tabulated in Table 4.

Again, the quadrupolar splitting frequencies of both isotopes are only about 10% smaller than the estimates along the scaling factors given above. On the other hand, the magnetic hyperfine field is increased even by almost 80% compared to the simple conversion, and its anisotropic contribution is clearly larger than for the $^{73}$Ge(3) nucleus and is even inverted in sign.

The signals of $^{69}$Ga and $^{71}$Ga at the Ge(1) sites occupied only to a minor extend (about 14%), instead of the preferentially occupied Ge(2) site [15], are encountered in the 120–230 MHz range, peaked in the 130–150 MHz range due to the $\theta_{min}/\theta_{max}(x = 0.4, 0.7)$ or domain and wall edge ($x = 1.0$) contributions, but they are generally very weak due to their large spectral spread and the low site occupation. Thus a comparison with simulated spectra was reasonable only for the enhanced signal strength of the $x = 1.0$ wall signals [28]. The large hyperfine anisotropy of the Ge(1) site is confirmed and the low frequency wing of the $^{55}$Mn signal (Fig. 9a) is accounted for by the $^{71}$Ga contribution, as mentioned in Section 4.4. Parameters are given in Table 4.

**Table 4.** NMR parameters of $^{69,71}$Ga on the Ge sites in $LuMn_6Ge_{6-x}Ga_x$ at $T = 4.2$ K.

| | Ge(1) | Ge(2) | Ge(3) |
|---|---|---|---|
| $x = 0.4$ | | | |
| $^{69}\Delta\nu_Q$/MHz | | 9.0(5) | 30.0(5) |
| $^{69}\nu_{is}$/MHz | | 90.7(4) | 242.6(10) |
| $^{69}\nu_{an}$/MHz | | 24.8(4) | −19.1(10) |
| $^{71}\Delta\nu_Q$/MHz | | 6.0(5) | 19.1(5) |
| $^{71}\nu_{is}$/MHz | | 113.0(4) | 309.1(15) |
| $^{71}\nu_{an}$/MHz | | 31.0(4) | −24.3(15) |
| $x = 0.7$ | | | |
| $^{69}\Delta\nu_Q$/MHz | | 9.0(5) | 30.0(5) |
| $^{69}\nu_{is}$/MHz | | 88.9(4) | 237.8(10) |
| $^{69}\nu_{an}$/MHz | | 25.1(4) | −22.8(10) |
| $^{71}\Delta\nu_Q$/MHz | | 6.0(5) | 19.1(5) |
| $^{71}\nu_{is}$/MHz | | 109.2(4) | 302.8(15) |
| $^{71}\nu_{an}$/MHz | | 30.8(4) | −29.0(15) |
| $x = 1.0$ | | | |
| $^{69}\Delta\nu_Q$/MHz | 18.0(16) | 9.0(5) | 30.0(5) |
| $^{69}\nu_{is}$/MHz | 106.7(13) | 91.2(4) | 234.4(20) |
| $^{69}\nu_{an}$/MHz | −106.7(13) | 29.9(4) | −18.4(20) |
| $^{71}\Delta\nu_Q$/MHz | 11.4(10) | 6.0(5) | 19.1(5) |
| $^{71}\nu_{is}$/MHz | 135.3(17) | 115.3(4) | 302.0(15) |
| $^{71}\nu_{an}$/MHz | −135.3(17) | 37.7(4) | −23.7(15) |

## 5 Discussion

The series of pseudo-ternary intermetallic compounds $LuMn_6Ge_{6-x}Ga_x$ ($0 \le x \le 1$) is an ideal model system for the study of the influence of long range exchange interaction (parameters $B_1$ and $B_2$ in Fig. 1c) between ferromagnetically coupled layers (Kagomé net planes) of manganese moments of about $2.1\,\mu_B$ on the macroscopic magnetic properties [9,22]. Growth of the lattice constant $c$ with Ga content $x$ is paralleled by the sequence of antiferromagnetic ($x = 0$), helimagnetic ($x = 0.4$ and 0.7) and ferromagnetic ($x = 1.0$) arrangement in the low-temperature range, a clear evidence for $|B_2|$ becoming larger than $|B_1/4|$.

The variation of the magnetic anisotropy energy $E_A$ has to be considered as well. A 10% anisotropy of the manganese hyperfine field at the $^{55}$Mn nucleus was derived earlier, see Section 2 [11]. The inclined flat spiral magnetic structure of the $x = 0.4$ and 0.7 compounds with $\theta^*_{\perp \mathrm{Mn}} \approx 45°$ indicates that $|K_1| \approx |K_2|$, with $K_1 < 0 < K_2$ in equations (1) and (2), see Figure 2. The magnetic anisotropy varies with $x$. A decrease of the value $|K_2|$ with increasing $x$ is in accordance with $\theta_{\mathrm{Mn}} = 55°$ in the ferromagnetic $x = 1.0$ ($x_{mp} = 0.84$) compound (i.e. $K_2/K_1 \approx -0.75$). The anisotropy energy is then lower for $\theta = 90°$ than for $\theta = 0°$ (Fig. 2), explaining that the domain wall center corresponds to $\theta_{\mathrm{Mn}} = 90°$, not $\theta_{\mathrm{Mn}} = 0°$. This was one result of the NMR lineshape analysis for the wall signals in $LuMn_6Ge_5Ga_1$, Sections 4.3 and 4.5. The continuity of the variation of the anisotropy supports a remaining deviation of the preferred direction of the antiferromagnet $LuMn_6Ge_6$ from $\theta_{\mathrm{Mn}} = 0$ as well. Such a small canting or double cone structure for the A-A-B-B-sequence in zero field at 4.2 K by about 5° had to be concluded in Section 4.2 from the Lutetium NQR/NMR spectrum. In these respects, the NMR results presented above support and complement the earlier picture of $LuMn_6Ge_{6-x}Ga_x$ primarily based on neutron scattering data and magnetization measurements. We presented one of the rare examples where all elements and all structural sites could be monitored by appropriate, naturally abundant $I \ge 3/2$ NMR isotopes (Tab. 2), in the case of Ga even by two isotopes differing in magnetic and quadrupolar moment. The assignment of the three Ge sites Ge(1), Ge(2) and Ge(3) (Fig. 1) required the use of ab initio electric field gradient calculations, but all other analyses required only the correct description of the variety of the experimental spectra, Figures 6–11. Consistency of the analysis is guaranteed by the systematic variation of the parameters compiled in Tables 3 and 4 for varied Ga content $x$, and by the correlation of $^{73}$Ge and $^{69,71}$Ga results as well as the mutual agreement of the $^{69}$Ga and $^{71}$Ga results. The main disadvantage of the presented comprehensive NMR analysis was evidently the time consumption that resulted from the fact that an extremely broad frequency range of 6–350 MHz had to be measured, and most of the spectra had to be unravelled by comparison with simulations requiring the weighted superposition of angular dependent spectra that had to be calculated by exact diagonalization of the appropriate Hamiltonian.

Five results of this analysis merit special attention.

(i) The small variation of the $^{55}$Mn hyperfine field with $x$ indicates a rather small variation of the Mn moment with $x$, i.e. $\mu_{\mathrm{Mn}} = 2.14\,\mu_B, 2.19(4)\,\mu_B, 2.15(1)\,\mu_B$ and $2.05(4)\,\mu_B$ for $x = 0, 0.4, 0.7$ and 1.0 respectively (see Sect. 4.4). This is further supported by the rather small variation of the isotropic part of the $^{73}$Ge or $^{71,69}$Ga hyperfine field at the Ge(2) and Ge(3) sites with $x$, which is below 6%, increasing with $x$ for the Ge(2) site and decreasing for the Ge(3) site.

(ii) There is an at least qualitative correlation between Mn-Ge separation and hyperfine field. The Ge(2) sites have the largest separation from their nearest six Mn neighbours, which belong all to the same Kagomé net plane (Figure 1). For these sites, $^{73}$Ge or $^{69,71}$Ga nuclei sense the smallest transferred magnetic hyperfine interaction. For the Ge(1) and Ge(3) sites, residing in the middle between two different Kagomé planes, the separation from the $2 \times 3$ Mn nearest neighbours is similar and substantially smaller (by 7%), and the transferred hyperfine field is larger. It is important to note that the transferred field at the Ge(3) site is larger than that at the Ge(1) site, in spite of a 0.9–1.5% larger separation. This must be related to the fact that Ge(3) resides in the middle of the Mn-Ge(2)-Ge(3)-Ge(2)-Mn double layer exhibiting ferromagnetic coupling (Figs. 1b and 1c), whereas the exchange interaction of the Mn-(Lu, Ge(1))-Mn double layer

(Fig. 1) is much weaker, allowing for large canting or antiferromagnetic arrangements in dependence of $x$.

(iii) The anisotropy of the hyperfine interaction at the Ge and Ga sites varies with the distance from the rare earth plane. For the Ge(3) [or Ga(3)] sites, the anisotropic part $\nu_{an}$ amounts only to about +0.7% [−8%] of the isotropic part $\nu_{is}$, for the Ge(2) [and Ga(2)] sites, this ratio rises to about +25% [+29%], and for the Ge(1) [Ga(1)] sites to −64% [−100%]. Evidently the strength of the electric field gradient and the relative strength of the magnetic hyperfine anisotropy are not correlated. At all three Ge sites, the relative anisotropy of the magnetic hyperfine field is larger for Ga nuclei than for Ge nuclei.

(iv) The Ge(1) site is most sensitive to the varying arrangement of the Mn moments in subsequent Kagomé net double layers in $LuMn_6Ge_{6-x}Ga_x$. Thus, for $x = 0$, the $^{73}$Ge resonances of the canted antiferromagnet occur at very low frequency, below the range of our analysis. The highest value of the isotropic part of the hyperfine field is reached for the long spiral at $x = 0.7$. No further increase of $^{73}\nu_{is}$ is observed for the ferromagnetic arrangement at $x = 1.0$, probably because in this compound the absolute value of the Mn moment is reduced compared to the antiferromagnetic and helimagnetic compounds, as is indicated by neutron scattering as well as $^{55}$Mn NMR frequency analysis.

(v) It is evident that the substitution of Ga for Ge in $LuMn_6Ge_{6-x}Ga_x$ influences the long range exchange interaction ($B_1, B_2$ in Fig. 1c) whilst causing a small increase of the lattice constant $c$. Thus the weak antiferromagnetic coupling $A_3$ is overcompensated, and spiral or ferromagnetic arrangements are favored for $x$ growing from 0 to 1. It is interesting to consider the local differences between Ge and Ga nuclei at the three inequivalent lattice sites. We have shown that the charge distribution is not much changed with $x$, because the electric field gradients felt by Ge or Ga nuclei are the same within 10%. On the other hand, we have seen that the spin polarization of the conduction or bonding electrons is considerably enhanced at the Ga sites compared to the Ge sites, because the magnetic hyperfine fields of $^{69,71}$Ga at the Ge(1), Ge(2) and Ge(3) sites were 35–80% larger than according to a simple conversion with the tabulated parameters of the different elements and isotopes (Sect. 4.5). This is thus the most pronounced change accompanying the substitution of Ga for Ge in $LuMn_6Ge_{6-x}Ga_x$. We assume that this increase in the spin polarization (v) and anisotropy (iii) is related with the variation of the magnetic order with the Ga content in $LuMn_6Ge_{6-x}Ga_x$.

It is interesting to focus on the anisotropy of the spin polarization and hyperfine interaction at the Ge(1) (and Ga(1)) sites, reflecting the interactions within the Mn-(Lu, Ge(1))-Mn double layer. The minimum values are obtained for Mn moment direction parallel to the $c$ direction (even zero for Ga(1)), the maximum values for moments in the Kagomé net plane. This angular dependence must have its effect on the overall magnetic order of $LuMn_6Ge_{6-x}Ga_x$, because the Mn moment direction rotates away from the $c$ direction for growing Ga content $x$.

## 6 Concluding remarks

As the final goal in a sequence of studies of $RMn_6Ge_6$ compounds with macroscopic, field- and temperature variable magnetization measurements and local probing by zero-field NMR of all accessible nuclear isotopes, we focused on the $LuMn_6Ge_{6-x}Ga_x$ pseudo-ternary compounds ($0 \leq x \leq 1$). Using magnetically well defined samples we could monitor the local variations accompanying the sequence from antiferromagnetic (double cone) order for $x = 0$, over helimagnetism (or inclined flat spiral) for $x = 0.4$ and 0.7, to ferromagnetic arrangement for $x = 1.0$. The $^{175}$Lu NMR spectrum was of decisive importance for the proof of the canted or double cone structure in $LuMn_6Ge_6$ at 4.2 K. The $^{55}$Mn NMR signals showed that the local Mn moment of about 2.1 $\mu_B$ varies by less than ±5% in the sequence of compounds. The assignment and analysis of the $^{73}$Ge NMR spectra for the three structurally inequivalent sites Ge(1), Ge(2) and Ge(3) was successfully accomplished. The different degrees of hyperfine anisotropy and the most pronounced sensitivity of the Ge(1) site to the overall magnetic structure have to be stressed. The NMR spectra of both gallium isotopes $^{69}$Ga and $^{71}$Ga at the three sites Ge(1), Ge(2) and Ge(3) could be detected, quantitatively described and correlated with the respective $^{73}$Ge data. The $^{69,71}$Ga spectra for the Ge(3) site are most easily observed, because the anisotropy of the magnetic hyperfine interaction of this site is the smallest and the measuring frequency is the highest. However, the $^{69,71}$Ga spectra for the preferred Ge(2) site could also clearly be resolved already for the low $x$ value $x = 0.4$, in spite of its 2.5 times lower resonance frequency.

According to our earlier molecular field analysis, in order to outweigh the antiferromagnetic exchange coupling ($A_3$ in Fig. 1c) of the Mn-(Lu, Ge(1))-Mn double layer to give rise to helimagnetic or ferromagnetic long range order in $LuMn_6Ge_{6-x}Ga_x$ for $x = 0.4$ and 0.7, or 1.0, respectively, the long range exchange parameters $B_1$ and especially $B_2$ must increase. An increase of the conduction and bonding electron spin polarization at the Ga nuclei compared to the Ge nuclei by 35–80% could indeed be proved in this analysis.

We thank Sandra Drotziger and Marc Uhlarz for experimental contributions and K.H.J. Buschow for making the $LuMn_6Ge_6$ sample available to us.

## References

1. E. Dormann, in *Handbook on the Physics and Chemistry of Rare Earths*, edited by K.A. Gschneidner Jr, (Le Roy Eyring, North-Holland, 1991), Vol. **14**, p. 63, and references therein
2. H. Nakamura, M. Shiga, J. Alloys Compounds **326**, 157 (2001)
3. P. Rösch, M.T. Kelemen, B. Pilawa, E. Dormann, K.H.J. Buschow, J. Magn. Magn. Mater. **164**, 175 (1996)

4. P. Rösch, J. Weizenecker, M.T. Kelemen, J. Ruf. C. Zobel, E. Dormann, J. Magn. Magn. Mater. **177–181**, 1071 (1998)
5. M.T. Kelemen, P. Rösch, E. Dormann, K.H.J. Buschow, J. Magn. Magn. Mater. **188**, 195 (1998)
6. P. Rösch, M.T. Kelemen, E. Dormann, G. Tomka, P.C. Riedi, J. Phys. Condens. Matt. **12**, 1065 (2000)
7. M.T. Kelemen, P. Rösch, N. Kaplan, E. Dormann, Eur. Phys. J. B **18**, 435 (2000)
8. M.T. Kelemen, Ch. Sürgers, E. Dormann, J. Magn. Magn. Mater. **226–230**, 1188 (2001)
9. M.T. Kelemen, P. Rösch, E. Dormann, K.J.H. Buschow, J. Magn. Magn. Mater. **223**, 253 (2001)
10. M.T. Kelemen, M.S.S. Brooks, E. Dormann, J. Phys. Condens. Matt. **13**, 657 (2001)
11. M.T. Kelemen, P. Rösch, E. Dormann, Phys. Lett. A **279**, 275 (2001)
12. P. Rösch, Ph.D. thesis, Universität Karlsruhe (1997, unpublished)
13. T. Mazet, R. Welter, G. Venturini, E. Ressouche, B. Malaman, Solid State Commun. **110**, 407 (1999)
14. G. Venturini, J. Alloys. Compounds **309**, 20 (2000)
15. G. Venturini, A. Vernière, B. Malaman, J. Alloys. Compounds **319**, 22 (2001)
16. C. Lefèvre, G. Venturini, B. Malaman, J. Alloys. Compounds **343**, 38 (2002)
17. C. Lefèvre, G. Venturini, B. Malaman, J. Alloys. Compounds **354**, 47 (2003)
18. M. Koyama, Y. Narumi, S. Yoshii, K. Kindo, L. Zhang, E. Brück, K.H.J. Buschow, F.R. de Boer, C. Lefèvre, G. Venturini, J. Alloys Comp. **408–412**, 161 (2006)
19. L. Zhang, J.C.P. Klaasse, E. Brück, K.H.J. Buschow, F.R. de Boer, S. Yoshii, K. Kindo, C. Lefèvre, G. Venturini, Phys. Rev. B **70**, 224425 (2004)
20. F. Canepa, M. Napoletano, C. Lefèvre, G. Venturini, J. Alloys Compounds **339**, 26 (2002)
21. P. Schobinger-Papamantellos, G. Andre, J. Rodriguez-Carvajal, J.H.V.J. Brabers, K.H.J. Buschow, J. Alloys Compounds **226**, 113 (1995)
22. M.T. Kelemen: *Magnetische Ordnung und Hyperfeinwechselwirkung in ternären Seltenerd-Mangan-Germanium-Verbindungen*, Ph.D. thesis, Universität Karlsruhe 1999 (Cuvillier-Verlag Göttingen, 1999)
23. P. Pyykkö, Molec. Phys. **19**, 1617 (2001)
24. P. Blaha, K. Schwarz, P.H. Dederichs, Phys.Rev. B **37**, 2792 (1988)
25. P. Blaha, K. Schwarz, G.K.H. Madsen, D. Kvasnicka, J. Luitz, *WIEN2k, An augmented Plane Wave + Local Orbitals Program for Calculating Crystal Properties* (Karlheinz Schwarz, Techn. Universität Wien, Austria, 2001)
26. T.P. Das, E.L. Hahn, in *Nuclear Quadrupole Resonance Spectroscopy, Solid State Physics*, Suppl. 1, edited by F. Seitz, D. Turnbull (Academic Press, New York, 1958)
27. G.C. Carter, L.H. Bennett, D.J. Kahan, in *Progress in Materials Science 20*, edited by B. Chalmers, J.W. Christian, T.B. Massalski, Part I (1977), p. 79
28. J. Schnelzer, Ph.D. thesis, Universität Karlsruhe (2007, unpublished)
29. R. Montbrun, Diplomarbeit, Universität Karlsruhe (2006, unpublished)